

Novel LHC signature of Type-II seesaw model

Dilip Kumar Ghosh
School of Physical Sciences
IACS, Kolkata



November 12, 2018

Outline

Based on the work: **PRD 97, 115022 (2018)**
DKG, Nivedita Ghosh, Ipsita Saha, Avirup Shaw

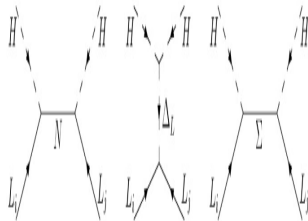
- 1 Motivation
- 2 Model
- 3 Theoretical And Experimental Constraints
- 4 Analysis
- 5 Conclusion

Motivation

- Neutrinos are massless in the SM.
- Different experimental data on neutrino sector \implies neutrinos have tiny mass
- The simplest way to obtain non-zero neutrino masses is by breaking the global $(B - L)$ symmetry of the SM
- One classic solution \implies Seesaw Mechanism
- This is a realization of the effective dimension-5 Weinberg operator using only renormalizable interactions.
- The effective Weinberg operator is $\implies y_{ij}(L_i^T \Phi)(L_j^T \Phi)/M$, M is a heavy new physics scale. [Ref: S. Weinberg (79)]

Motivation

- Three types of Seesaw mechanisms have been proposed :
 - Type I : SM + right-handed heavy neutrino
 - Type II : SM + $SU(2)_L$ triplet ($Y = 2$) scalar
 - Type III : SM + $SU(2)_L$ triplet ($Y = 0$) fermion



[Ref: P. Minkowski (77), T. Yanagida, Gell-Mass, Ramond and Slansky (79), Mohapatra and Senjanovic (80); J. Schechter and Valle (80), Magg and Wetterich (80); Foot, He and Joshi, (89).]

- In this talk we will focus on Type II Seesaw model.
- Constraints on model parameters from the vacuum stability and perturbative unitarity of this model.
- Predictions at the current and future run of the LHC.

Model

Type-II seesaw model contains an $SU(2)_L$ triplet scalar field Δ with hypercharge $Y = 2$ in addition to the SM fields.

$$\Delta = \frac{\sigma^j}{\sqrt{2}} \Delta_j = \begin{pmatrix} \delta^+/\sqrt{2} & \delta^{++} \\ \delta^0 & -\delta^+/\sqrt{2} \end{pmatrix}, \quad (1)$$

where $\Delta_1 = (\delta^{++} + \delta^0)/\sqrt{2}$, $\Delta_2 = i(\delta^{++} - \delta^0)/\sqrt{2}$, $\Delta_3 = \delta^+$.

The complete Lagrangian of this scenario is given by:

$$\mathcal{L} = \mathcal{L}_{\text{Yukawa}} + \mathcal{L}_{\text{Kinetic}} - V(\Phi, \Delta), \quad (2)$$

where the kinetic and Yukawa interactions are respectively.

$$\mathcal{L}_{\text{kinetic}} = (D_\mu \Phi)^\dagger (D^\mu \Phi) + \text{Tr} \left[(D_\mu \Delta)^\dagger (D^\mu \Delta) \right], \quad (3)$$

$$\mathcal{L}_{\text{Yukawa}} = \mathcal{L}_{\text{Yukawa}}^{\text{SM}} - (Y_\Delta)_{ij} L_i^\top C i \sigma_2 \Delta L_j + \text{h.c.} \quad (4)$$

Here $\Phi^\top = (\phi^+ \quad \phi^0)$ is the SM scalar doublet.

$$D_\mu \Delta = \partial_\mu \Delta + i \frac{g}{2} [\sigma^a W_\mu^a, \Delta] + ig' B_\mu \Delta \quad (a = 1, 2, 3). \quad (5)$$

Model

The most general scalar potential¹ is given as :

$$V(\Phi, \Delta) = -m_\Phi^2(\Phi^\dagger\Phi) + \frac{\lambda}{4}(\Phi^\dagger\Phi)^2 + M_\Delta^2 \text{Tr}(\Delta^\dagger\Delta) + \left(\mu\Phi^\dagger i\sigma_2\Delta^\dagger\Phi + \text{h.c.}\right) + \lambda_1(\Phi^\dagger\Phi)\text{Tr}(\Delta^\dagger\Delta) + \lambda_2 \left[\text{Tr}(\Delta^\dagger\Delta)\right]^2 + \lambda_3\text{Tr}(\Delta^\dagger\Delta)^2 + \lambda_4\Phi^\dagger\Delta\Delta^\dagger\Phi. \quad (6)$$

After the EWSB, the minimization of the potential calculates the two mass parameters as,

$$m_\Phi^2 = \lambda \frac{v_d^2}{4} - \sqrt{2}\mu v_t + \frac{(\lambda_1 + \lambda_4)}{2} v_t^2, \quad (7)$$

$$M_\Delta^2 = \frac{\mu v_d^2}{\sqrt{2}v_t} - \frac{\lambda_1 + \lambda_4}{2} v_d^2 - (\lambda_2 + \lambda_3)v_t^2, \quad (8)$$

The triplet vev (v_t) contributes to the electroweak gauge boson masses M_W^2 and M_Z^2 at tree level, $M_W^2 = \frac{g^2(v_d^2+2v_t^2)}{4}$ and $M_Z^2 = \frac{g^2(v_d^2+4v_t^2)}{4\cos^2\theta_W}$ respectively. The SM ρ -parameter is given by:

$$\rho = \frac{M_W^2}{M_Z^2 \cos^2\theta_W} = \frac{1 + \frac{2v_t^2}{v_d^2}}{1 + \frac{4v_t^2}{v_d^2}}. \quad (9)$$

¹A. Arhrib et al, PhysRevD.84.095005

model

One gets an upper bound on $\frac{v_t}{v_d} < 0.02$ or $v_t < 5$ GeV.

After EWSB, the scalar fields expanded around respective vevs, can be parameterized as

$$\Phi = \frac{1}{\sqrt{2}} \begin{pmatrix} \sqrt{2}\chi_d^+ \\ v_d + h_d + i\eta_d \end{pmatrix} \quad \Delta = \frac{1}{\sqrt{2}} \begin{pmatrix} \delta^+ & \sqrt{2}\delta^{++} \\ v_t + h_t + i\eta_t & -\delta^+ \end{pmatrix} \quad (10)$$

As a consequence, the scalar spectrum contains seven physical Higgs bosons: two doubly charged $H^{\pm\pm}$, two singly charged H^\pm , two CP-even neutral (h, H) and a CP-odd (A) Higgs particles.

The corresponding mixing angles are given as

$$\tan \beta' = \frac{\sqrt{2}v_t}{v_d}, \quad \tan \beta = \frac{2v_t}{v_d} \equiv \sqrt{2} \tan \beta' \quad (11a)$$

$$\text{and } \tan 2\alpha = \frac{2\mathcal{B}}{\mathcal{A} - \mathcal{C}}, \quad (11b)$$

$$\text{where, } \mathcal{A} = \frac{\lambda}{2}v_d^2, \quad \mathcal{B} = v_d[-\sqrt{2}\mu + (\lambda_1 + \lambda_4)v_t], \quad \mathcal{C} = \frac{\sqrt{2}\mu v_d^2 + 4(\lambda_2 + \lambda_3)v_t^3}{2v_t} \quad (11c)$$

$$\lambda = \frac{2}{v_d^2} (c_\alpha^2 m_h^2 + s_\alpha^2 m_H^2), \quad (12a)$$

$$\lambda_1 = \frac{4m_{H^\pm}^2}{v_d^2 + 2v_t^2} - \frac{2m_A^2}{v_d^2 + 4v_t^2} + \frac{\sin 2\alpha}{2v_d v_t} (m_h^2 - m_H^2), \quad (12b)$$

$$\lambda_2 = \frac{1}{v_t^2} \left[\frac{1}{2} (s_\alpha^2 m_h^2 + c_\alpha^2 m_H^2) + \frac{1}{2} \frac{v_d^2 m_A^2}{v_d^2 + 4v_t^2} - \frac{2v_d^2 m_{H^\pm}^2}{v_d^2 + 2v_t^2} + m_{H^\pm\pm}^2 \right], \quad (12c)$$

$$\lambda_3 = \frac{1}{v_t^2} \left[\frac{2v_d^2 m_{H^\pm}^2}{v_d^2 + 2v_t^2} - m_{H^\pm\pm}^2 - \frac{v_d^2 m_A^2}{v_d^2 + 4v_t^2} \right], \quad (12d)$$

$$\lambda_4 = \frac{4m_A^2}{v_d^2 + 4v_t^2} - \frac{4m_{H^\pm}^2}{v_d^2 + 2v_t^2}, \quad (12e)$$

$$\mu = \frac{\sqrt{2}v_t m_A^2}{v_d^2 + 4v_t^2}. \quad (12f)$$

Vacuum stability

$$\lambda \geq 0, \quad (13a)$$

$$\lambda_2 + \lambda_3 \geq 0, \quad (13b)$$

$$\lambda_2 + \frac{\lambda_3}{2} \geq 0, \quad (13c)$$

$$\lambda_1 + \sqrt{\lambda(\lambda_2 + \lambda_3)} \geq 0, \quad (13d)$$

$$\lambda_1 + \sqrt{\lambda \left(\lambda_2 + \frac{\lambda_3}{2} \right)} \geq 0, \quad (13e)$$

$$\lambda_1 + \lambda_4 + \sqrt{\lambda(\lambda_2 + \lambda_3)} \geq 0, \quad (13f)$$

$$\lambda_1 + \lambda_4 + \sqrt{\lambda \left(\lambda_2 + \frac{\lambda_3}{2} \right)} \geq 0. \quad (13g)$$

Perturbative unitarity

$$|\lambda_1 + \lambda_4| \leq 16\pi, (14a)$$

$$|\lambda_1| \leq 16\pi, (14b)$$

$$|2\lambda_1 + 3\lambda_4| \leq 32\pi, (14c)$$

$$|\lambda| \leq 32\pi, (14d)$$

$$|\lambda_2| \leq 8\pi, (14e)$$

$$|\lambda_2 + \lambda_3| \leq 8\pi, (14f)$$

$$|\lambda + 4\lambda_2 + 8\lambda_3 \pm \sqrt{(\lambda - 4\lambda_2 - 8\lambda_3)^2 + 16\lambda_4^2}| \leq 64\pi, (14g)$$

$$|3\lambda + 16\lambda_2 + 12\lambda_3 \pm \sqrt{(3\lambda - 16\lambda_2 - 12\lambda_3)^2 + 24(2\lambda_1 + \lambda_4)^2}| \leq 64\pi, (14h)$$

$$|2\lambda_1 - \lambda_4| \leq 16\pi, (14i)$$

$$|2\lambda_2 - \lambda_3| \leq 16\pi. (14j)$$

- Constraints from electroweak precision test:** The strongest bound comes from the T-parameter which imposes strict limit on the mass splitting between the doubly and singly charged scalars, $\Delta M \equiv |m_{H^{\pm\pm}} - m_{H^\pm}|$ which should be $\lesssim 50 \text{ GeV}^2$.
- Experimental bounds on scalar masses :**
 - Singly charged scalars:** The direct search on the singly charged scalar at the LEP II puts a limit on $m_{H^\pm} \geq 78 \text{ GeV}$.
 - For our benchmark points, $m_{H^\pm} \sim 173 - 180 \text{ GeV}$, and for this mass range, $t \rightarrow bH^\pm$ decay mode is kinematically suppressed \implies no experimental limit on m_{H^\pm} from the charged higgs search in $t \rightarrow bH^\pm$.
 - Heavy H/A search :** $gg \rightarrow \Phi$, where $\Phi \equiv H/A$.
 - In Type II seesaw model, interactions between quarks and triplet scalars happen via the doublet and triplet mixing, which is proportional to (v_t/v_d) .
 - For our benchmark points, $v_t = 3 \text{ GeV}$, $\sigma(pp(gg) \rightarrow H) \propto (v_t/v_d)^2 \sim \mathcal{O}(10^{-4})$.
 - $\sigma(pp \rightarrow H)^{\text{NNLOQCD+EW}} = 13 \text{ (fb)}$ at 13 TeV LHC for the best possible benchmark point and this is well below the current 95% CL bound on $\sigma(gg \rightarrow H) \times \text{BR}(H \rightarrow ZZ)(\text{pb}) - m_H \text{ (GeV)}$ plane by the ATLAS Collaboration. [Ref.[ATLAS-CONF-2016-016](#)]
 - One can draw similar conclusions for the A
 - The second dominant process for H production at the LHC is VV fusion.
 - The ATLAS collaboration provided 95% CL limit on $\sigma(\text{VBF} \rightarrow H) \times \text{BR}(H \rightarrow W^+W^-) \text{ (pb)} - m_H \text{ (GeV)}$ plane. [Ref:[ATLAS Collaboration, EPJC 78, 24 \(2018\)](#)].
 - Our benchmark points satisfy this limit also.

²E. J. Chun et al.,JHEP11(2012)106

- **Doubly charged scalar searches:**
- The collider bound on $H^{\pm\pm}$ mass is strongly depends on the triplet vev v_t .
- For $v_t < 10^{-4}$ GeV (corresponds to large Yukawa couplings) and assuming degenerate scalars, the doubly charged Higgs boson decays to like sign dilepton (LSD) $\ell^\pm \ell^\pm$ with almost 100% probability.
- From the direct search of the doubly charged Higgs boson at 13 TeV LHC run, the current lower bound at 95% CL on its mass is $m_{H^{\pm\pm}} > 700 - 800 \text{ GeV}^3$ depending upon the final state lepton flavor.
- For $v_t > 10^{-4}$ GeV (\rightarrow small Y_ν), the branching ratio into LSD decreases substantially and there are other several competing decay modes of $H^{\pm\pm}$ opens up: (if kinematically accessible)
- $H^{\pm\pm} \rightarrow W^\pm W^\pm$
- $H^{\pm\pm} \rightarrow W^\pm H^\pm$
- $H^{\pm\pm} \rightarrow H^\pm H^\pm$
- **Constraints from Higgs signal strength:** Our choice of benchmark points remain within the 2σ limit of the current experimental bound ($0.85^{+0.22}_{-0.20}$) of the Higgs to diphoton signal strength. [Current $\mu = 1.1^{+0.32}_{-0.3}$ from CMS-PAS-HIG-13-001.]

³ATLAS collaboration, ATLAS-CONF-2017-053

High Scale Stability

- To find the high-scale valid region of the parameter space, we analyse the one-loop RG running of all the scalar quartic coupling together with the gauge and Yukawa coupling from the EW to some high scale.
- We choose two values of the triplet vev $v_t = 1, 3$ GeV.
- For such a large value of v_t , we can ignore the effect of the running of neutrino Yukawa couplings (small) in the RGE.
- In our RGE analysis we scan the parameter space in the following range :

$$\begin{aligned}
 m_H(m_A) &\in \{m_h, 2000\} \text{GeV}, & \sin \alpha &\in \{-0.1, 0.1\} \\
 m_{H^\pm}(m_{H^{\pm\pm}}) &\in \{100, 2000\} \text{GeV}, & &
 \end{aligned} \tag{15}$$

- We fix $m_h = 125$ GeV, the EW vev (v) = 246 GeV. $M_t(\text{pole}) = 173$, for which the running mass is $m_t(M_t) = 164$ GeV.
- All the scalar couplings are then derived using set of equations (12) to set their boundary conditions at M_t and we run the full one-loop RGE from M_t to some high scale.
- We ensure that the stability (13) and perturbative unitarity (14) conditions do not violate at any scale during RG running.
- We have also impose the $\Delta M \equiv |m_{H^{\pm\pm}} - m_{H^\pm}|$ which should be $\lesssim 50$ GeV, from T -parameter.

- The requirement of absolute stability and unitarity entail a relation among the scalar mass parameters and not all of them remain independent.
- The conditions Eqs(13a) and (14f) when translated to mass terms using Eq.(12) $\implies m_A$ as a function of m_h and m_H and their mixing angle α and can be approximated as :

$$m_A^2 \simeq (m_H^2 \cos^2 \alpha + m_h^2 \sin^2 \alpha) \quad (16)$$

for $v_t \ll v_d$.

- Similarly, $m_{H^{\pm\pm}}$ can also be determined once we set the unitarity condition of Eq.(14j) in addition to the Eq.(16), gives an approximate relation : $(2m_{H^{\pm}}^2 - m_A^2)$
- We independently scan all the masses.
- At the end we found that the mass of m_A and $m_{H^{\pm\pm}}$ bear such relation to maintain the stability and unitarity constraints.

High Scale Stability

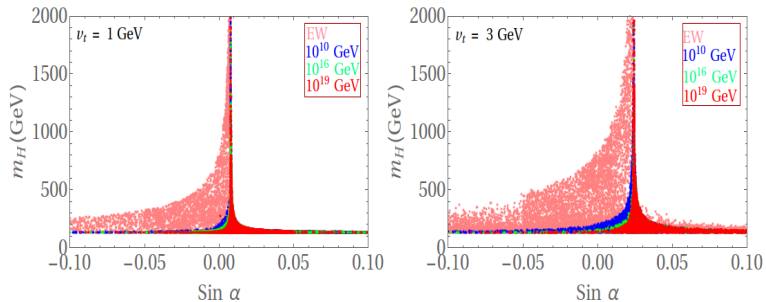


Figure: The valid parameter space in the $\sin \alpha - m_H$ plane for $v_t = 1$ GeV (left) and $v_t = 3$ GeV (right) for different values of cut-off scale.

- Significant amount of allowed parameter space at EW scale shrinks once we impose the stability of the vacuum all the way up to the Planck scale.
- Large value of heavy scalar masses happens only for a small non-zero value of $\sin \alpha$ when high scale stability is demanded and the absolute range of $\sin \alpha$ shifts toward more positive value if the triplet vev is increased from 1 to 3 GeV.
- This is a consequence of the unitarity bound Eq.(14 a).

High Scale Stability

- The relation among λ_s (Eq.(12)) and Eq.(14a) turns out to be

$$\frac{2m_A^2}{v_d^2 + 4v_t^2} + \frac{\sin 2\alpha}{2v_d v_t} (m_h^2 - m_H^2) < 16\pi. \quad (17)$$

- For $v_t \ll v_d$, and $m_A^2 \simeq (m_H^2 \cos^2 \alpha + m_h^2 \sin^2 \alpha)$, the limit is trivially satisfied for $\sin \alpha \simeq 2v_t/v_d$ reaching the decoupling limit of large $m_H (\gg m_h)$.
- This also means that in the SM-like limit (large $m_H \gg m_h$), the mixing angle tends to zero for $v_t \rightarrow 0$.
- An increase in v_t will shift the decoupling region for the non-standard scalars to large mixing angle.
- This feature is reflected in our analysis, where the peak of the allowed region is shifted for $v_t = 1$ GeV to 3 GeV to more larger $\sin \alpha$.

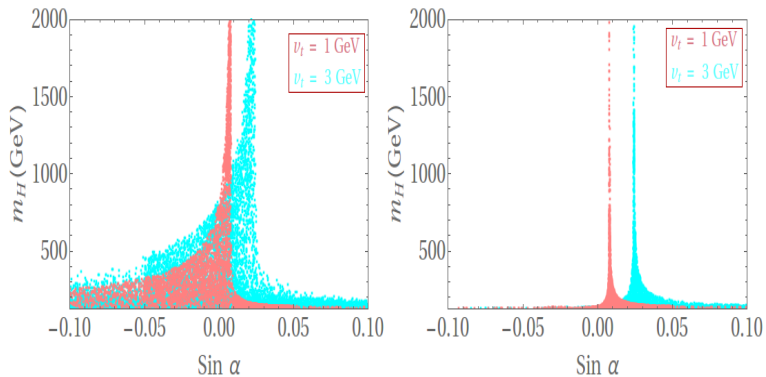


Figure: The valid parameter space in the $\sin \alpha - m_H$ plane for $\nu_t = 1$ GeV and 3 GeV at EW scale (left) and at the Planck scale (right)

- We now explore the parameter space available at the Planck scale allowed region in the LHC run and look for the prospect of novel signature of non-standard scalars.
- For $\sin \alpha \sim \mathcal{O}(0.1)$, Planck scale valid region only allows the heavier neutral scalar mass (m_H) close to the SM-like higgs mass m_h (degenerate scenario).
- T -parameter constraints push all other scalar masses ($m_A, m_{H^\pm}, m_{H^{\pm\pm}}$) in the same mass region. [see PRD 87, 015020 (2013)]
- We consider non-degenerate scenario, with triplet scalar masses around few hundred (200-300) GeV \implies ($0.01 < \sin \alpha < 0.05$) for $v_t = 3$ GeV.
- We investigate the signal of the associated production of the singly and doubly charged scalars for some specific final state.
- $m_{H^{\pm\pm}}$ in the high-scale stable parameter space is related to m_{H^\pm} and $m_{H(A)}$ as

$$m_{H^{\pm\pm}}^2 - m_{H^\pm}^2 \approx m_{H^\pm}^2 - m_A^2 (m_H^2) \quad (18)$$

- Two different mass hierarchy among heavy triplet scalars :
 - Positive scenario ($\lambda_4 > 0$) :: $m_{H^{\pm\pm}} < m_{H^\pm} < m_A/m_H$.
 - Negative scenario ($\lambda_4 < 0$) :: $m_{H^{\pm\pm}} > m_{H^\pm} > m_A/m_H$.

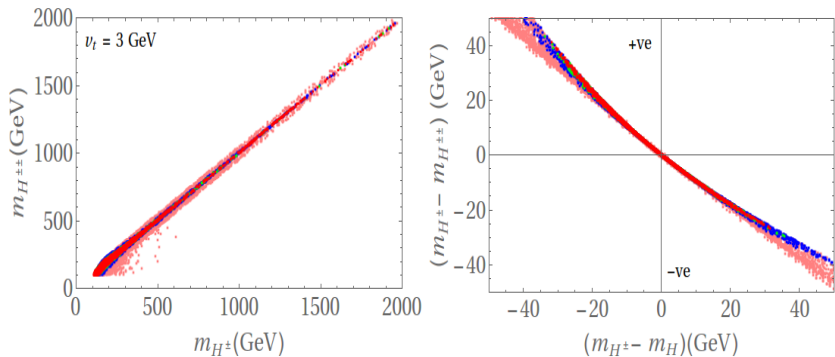


Figure: (Left panel) The allowed parameter space in the $m_{H^\pm} - m_{H^{\pm\pm}}$ plane for triplet vev $v_t = 3 \text{ GeV}$. The different colors follow the same convention as in Fig. 2. (Right panel) The corresponding allowed parameter space to show the relation between the mass splittings of the singly charged Higgs to the neutral Higgs ($m_{H^\pm} - m_H$) and singly charged Higgs to the doubly charged Higgs ($m_{H^\pm} - m_{H^{\pm\pm}}$). The upper left square corresponds to the valid region for our positive scenario while the lower right corner denotes the same but for our negative scenario.

Collider Analysis

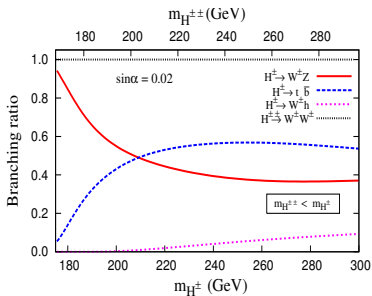


Figure: Branching ratio of different two body decay modes for the doubly charged and singly charged scalars for $\sin \alpha = 0.02$ and $v_t = 3$ GeV for the positive scenario.

- Only positive scenario has been shown.
- We only show mass ranges for which $H^{\pm} \rightarrow W^{\pm}Z$ decays onshell.
- For $m_{H^{\pm}} \sim (170 - 200)$ GeV, $H^{\pm} \rightarrow W^{\pm}Z$
- $H^{\pm\pm} \rightarrow W^{\pm}W^{\pm}$ with 100% probability ($v_t = 3$ GeV).

Collider Analysis

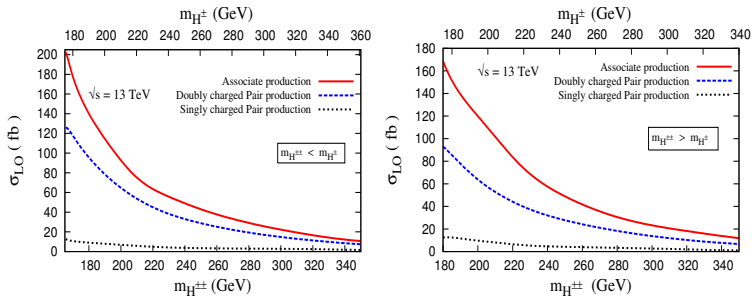


Figure: Left (Right) panel shows the variation of $\sigma_{LO}(pp \rightarrow H^{\pm\pm}H^{\mp})$ (fb) (solid red curve), $\sigma_{LO}(pp \rightarrow H^{++}H^{--})$ (fb) (blue dashed curve) and $\sigma_{LO}(pp \rightarrow H^{+}H^{-})$ (fb) (black dotted curve) with respect to charged Higgs masses at the LHC at $\sqrt{s} = 13 \text{ TeV}$ for positive (negative) scenario.

Benchmark Points

Mass Scenario	$\sin \alpha$	$m_{H^{\pm\pm}}$ (GeV)	m_{H^\pm} (GeV)	$m_H = m_A$ (GeV)	$\mu_{\gamma\gamma}$
Positive					
BP1	0.0220	165.48	173.25	180.70	0.79
BP2	0.0280	175.99	177.47	178.93	0.82
Negative					
BP1	0.0277	179.60	176.30	173.01	0.79
BP2	0.0300	184.17	180.11	175.95	0.81

Table: Benchmark points valid by the high-scale stability constraints up to the Planck scale and their corresponding Higgs to diphoton signal strength ($\mu_{\gamma\gamma}$) for both the positive and the negative scenario.

We consider the following two signal topologies:

- (i) $3\ell^\pm + \cancel{E}_T$;
- (ii) $(\ell^+\ell^+) + 4j + \cancel{E}_T$,

- For our analysis, both the signal and SM background events are generated at the LO parton level in Madgraph using the NNPDF3.0 parton distributions.
- The model has been implemented in FeynRules which gives the UFO model files required in madgraph.
- Pythia has been used for parton showering. Events are then passed through Delphes for detector effects.
- We consider the following SM processes in our analysis :
 - $t\bar{t} + \text{jets}$ (up to 3)
 - $t + 3\text{-jets}$
 - $V + 3\text{-jets}$, $V \equiv W^\pm, Z$
 - $VV + 3\text{-jets}$,
 - $W^\pm/Z/h$ and VVV
- SM background from top can be handled using the b -veto
- $W^\pm/Z + \text{jets}$ and $WW + \text{jets}$ with large production cross-sections can be suppressed with three lepton or same-sign dilepton criteria.
- Finally, the irreducible backgrounds left are the $WZ + \text{jets}$ and $t\bar{t} + (W/Z/h)$ with small effective cross-sections.

Basic cuts

In our signal and background events, we select jets and leptons using the following basic kinematical acceptance cuts :

$$\Delta R_{jj} > 0.6, \quad \Delta R_{\ell\ell} > 0.4, \quad \Delta R_{j\ell} > 0.7, \quad (19a)$$

$$\Delta R_{bj} > 0.7, \quad \Delta R_{b\ell} > 0.2, \quad (19b)$$

$$p_{T_{\min}}^j > 20 \text{ GeV}, \quad |\eta_j| < 5, \quad (19c)$$

$$p_{T_{\min}}^\ell > 10 \text{ GeV}, \quad |\eta_\ell| < 2.5, \quad (19d)$$

b-jet abiding by the efficiency as proposed by the ATLAS collaboration:

$$\epsilon_b = \begin{cases} 0 & p_T^b \leq 30 \text{ GeV} \\ 0.6 & 30 \text{ GeV} < p_T^b < 50 \text{ GeV} \\ 0.75 & 50 \text{ GeV} < p_T^b < 400 \text{ GeV} \\ 0.5 & p_T^b > 400 \text{ GeV} . \end{cases} \quad (20)$$

A mistagging probability of 10%(1%) for charm-jets (light-quark and gluon jets) are also included.

$$pp \rightarrow H^{++}H^- \rightarrow (W^+W^+) + (W^-Z) \rightarrow (\ell^+\ell^+) + \ell^- + \cancel{E}_T.$$

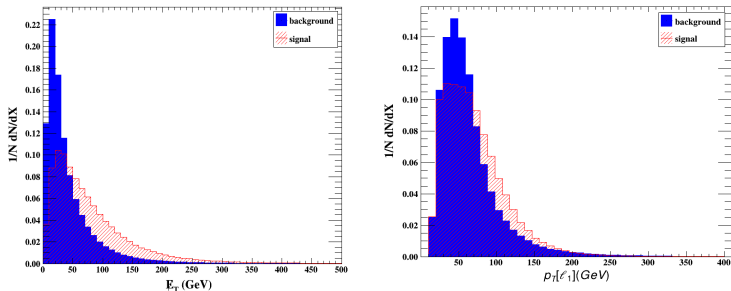


Figure: Normalized distribution of the (left panel) Missing transverse energy (\cancel{E}_T) and (right panel) the transverse momentum of the hardest lepton ($p_T(\ell_1)$) after the basic kinematical acceptance cuts for the benchmark BP1 of positive scenario.

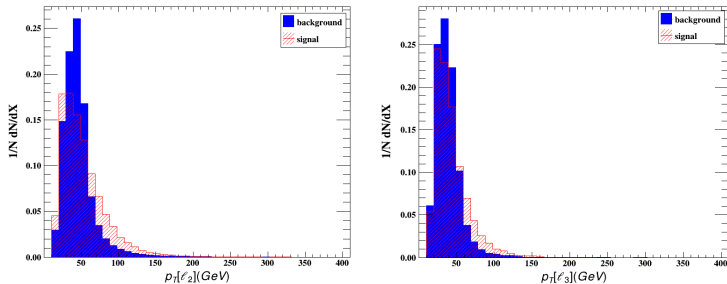


Figure: Transverse momentum (p_T) distribution (normalized) of the two sub-leading leptons for the benchmark BP1 of positive scenario.

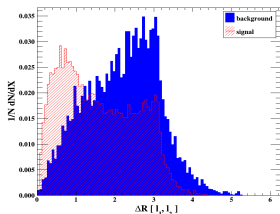


Figure: The $\Delta R(\ell_1^\pm \ell_2^\pm)$ distribution (normalized) between the two same-sign leptons for the positive scenario benchmark BP1.

- **(C1-1):** Our signal event is hadronically quiet, hence, we put a veto on any jet with $p_T > 30$ GeV.
- **(C1-2):** Next, to confirm the trilepton signature, we select at least three leptons with $p_T > 10$ GeV.
- **(C1-3):** For further affirmation of trilepton signature, we reject any additional charged lepton with $p_T > 10$ GeV.
- **(C1-4):** Furthermore, we claim that the same flavor opposite sign (SFOS) lepton invariant mass $M_{\ell^+\ell^-}$ should not lie between the window of 80-100 GeV to ensure that those are not directly produced from Z boson.

$3\ell^\pm + \cancel{E}_T$

- **(C1-5)**: Finally, our signal events are required to have $\cancel{E}_T > 30$ GeV.
- **(C1-6)**: The principal selection cut for the same-sign dilepton has been imposed. For this, we demand $\Delta R(\ell_1^\pm \ell_2^\pm) < 1.5$.

SM-background	Production Cross section (fb)	Effective cross section (fb) for background after the cut						
		C1-1	C1-2	C1-3	C1-4	C1-5	C1-6	
t+jets	2.22×10^5	157.50	0	0	0	0	0	
t \bar{t} +jets	7.07×10^5	420.37	0	0	0	0	0	
W^\pm +jets	1.54×10^8	4.96×10^7	0	0	0	0	0	
Z+jets	4.54×10^7	1.37×10^7	0	0	0	0	0	
W^+W^- +jets	8.22×10^4	4.76×10^3	0	0	0	0	0	
ZZ+jets	1.10×10^4	6.17×10^2	10.05	5.77	0.08	0.04	~ 0	
$W^\pm Z$ +jets	3.81×10^4	1.71×10^3	42.40	42.40	0.72	0.36	0.04	
W^+W^-Z	83.10	1.17	0.09	0.07	0.01	~ 0	0	
$W^\pm ZZ$	26.80	0.39	0.03	0.03	~ 0	0	0	
t \bar{t} + W^\pm	360	0.13	0.02	~ 0	0	0	0	
t \bar{t} + Z	585	0.15	0.02	0.01	~ 0	0	0	
t \bar{t} + h	400	0.02	~ 0	0	0	0	0	
Total SM Background	2.005×10^8	6.33×10^7	52.60	48.30	0.81	0.40	0.04	
Positive scenario	Production Cross section (fb)	Effective cross section (fb) for signal after the cut						Luminosity (in fb^{-1}) for 5σ significance
BP1	185.10	0.75	0.20	0.14	0.08	0.06	0.040	1250.0
BP2	158.70	0.65	0.16	0.11	0.06	0.05	0.034	1600.4
Negative scenario	Production Cross section (fb)	Effective cross section (fb) for signal after the cut						Luminosity (in fb^{-1}) for 5σ significance
BP1	153.80	0.63	0.16	0.11	0.06	0.05	0.033	1675.8
BP2	134.70	0.55	0.15	0.10	0.05	0.04	0.030	1944.4

Table: Effective cross section obtained after each cut for both signal ($3\ell^\pm + \cancel{E}_T$) and background and the respective required integrated luminosity for 5σ significance at 13 TeV LHC.

$3\ell^\pm + \cancel{E}_T$

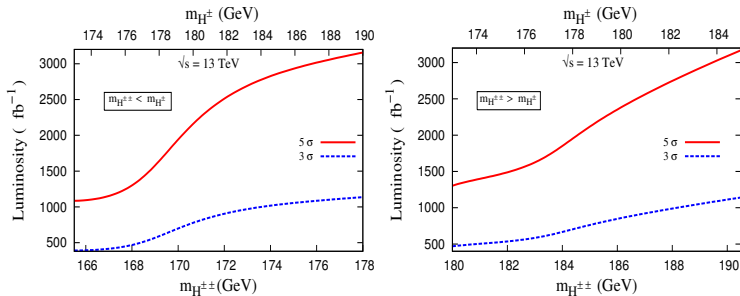


Figure: Left (Right) panel shows the required integrated luminosity for $3\ell^\pm + \cancel{E}_T$ final state with respect to charged Higgs masses at the LHC at $\sqrt{s} = 13$ TeV for positive (negative) scenario. The solid red coloured and blue coloured dashed curve correspond to constant signal significance at 5σ and 3σ respectively.

$2\ell^\pm + 4j + \cancel{E}_T$

$$\begin{aligned}
 pp \rightarrow H^{++}H^{--} &\rightarrow (W^+W^+) + (W^-W^-) \rightarrow (\ell^+\ell^+) + 4j + \cancel{E}_T \\
 pp \rightarrow H^{++}H^- &\rightarrow (W^+W^+) + (W^-Z) \rightarrow (\ell^+\ell^+) + 4j + \cancel{E}_T.
 \end{aligned}
 \tag{21}$$

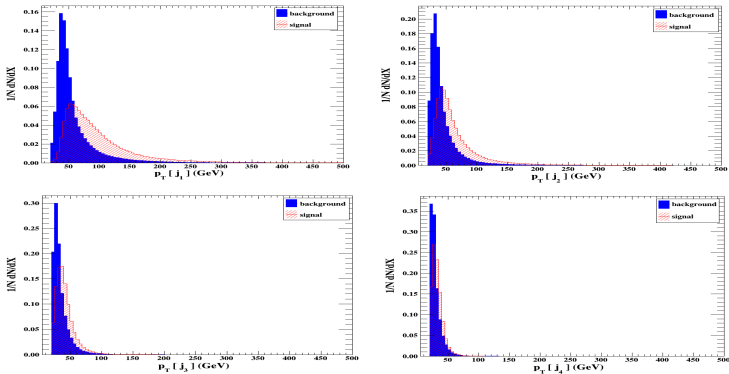


Figure: Transverse momentum (p_T) distribution (normalized) of the four leading jets for the final state $2\ell^\pm + 4j + \cancel{E}_T$ for the benchmark BP1 of positive scenario.

$$2\ell^\pm + 4j + \cancel{E}_T$$

- (C2-1): As explained, our signal is exempted from any b -jets, hence we can safely reject events with b -tagged jets of $p_T(b) > 40$ GeV.
- (C2-2): To guarantee that only 4 jets are present in the events, we reject any additional jets with $p_T(j_5) > 20$ GeV.
- (C2-3): Our signal also contains two isolated charged lepton and thus a veto on any additional leptons with $p_T > 10$ GeV is applied.
- (C2-4): Now, from the jet distribution, we choose the p_T of the leading jet to be at least greater than $p_T(j_1) > 60$ GeV.
- (C2-5): Moreover, for the next sub-leading jet we demand $p_T(j_2) > 40$ GeV to further subdue the background events.

$2\ell^\pm + 4j + \cancel{E}_T$

- (C2-6): A decent selection cut on the missing transverse energy is then applied as $\cancel{E}_T > 30$ GeV.
- (C2-7): Finally, the principal selection cut for the same-sign dilepton has been imposed. For this, we demand $\Delta R(\ell_1^\pm \ell_2^\pm) < 1.5$.

		Effective cross section (fb) after the cut							
SM-background	Production Cross section (fb)	C2-1	C2-2	C2-3	C2-4	C2-5	C2-6	C2-7	
$t\bar{t}$ +jets	2.22×10^5	8.46×10^4	8.01×10^4	8.01×10^4	4.89×10^4	3.44×10^4	1.54×10^4	0	
$t\bar{t}$ +jets	7.07×10^5	1.58×10^5	1.23×10^5	1.23×10^5	9.92×10^4	8.15×10^4	5.58×10^4	0	
W^\pm +jets	1.54×10^8	1.52×10^8	1.52×10^8	1.52×10^8	1.24×10^7	8.17×10^6	1.75×10^6	0	
Z+jets	4.54×10^7	4.27×10^7	4.27×10^7	4.27×10^7	3.76×10^6	2.48×10^6	4.65×10^5	0	
W^+W^- +jets	8.22×10^4	7.84×10^4	7.55×10^4	7.55×10^4	3.48×10^4	2.39×10^4	1.04×10^4	0	
ZZ+jets	1.10×10^4	8.96×10^3	8.67×10^3	8.65×10^3	4.27×10^3	2.89×10^3	1.16×10^3	0.05	
$W^\pm Z$ +jets	3.81×10^4	3.33×10^4	3.13×10^4	3.12×10^4	1.67×10^4	1.18×10^4	5.76×10^3	1.68	
$t\bar{t} + W^\pm$	360	78.00	55.15	55.00	47.00	39.80	33.00	0.13	
$t\bar{t} + Z$	585	110.00	68.20	67.00	59.60	52.04	44.30	0.04	
$t\bar{t} + h$	400	46.00	27.40	27.20	24.50	21.65	18.30	0.04	
Total SM Background	2.005×10^8	1.95×10^8	1.94×10^8	1.94×10^8	1.64×10^7	1.08×10^7	2.31×10^6	1.94	

		Effective cross section (fb) for signal after the cut							Luminosity (in fb^{-1}) for 5σ significance
Positive scenario	Production Cross section (fb)								
BP1	311.40	253.00	210.70	206.70	181.72	158.90	126.24	1.90	
BP2	259.30	211.23	175.92	172.64	151.75	132.66	105.42	1.55	

		Effective cross section (fb) for signal after the cut							Luminosity (in fb^{-1}) for 5σ significance
Negative scenario	Production Cross section (fb)								
BP1	246.23	200.00	166.50	163.32	143.61	125.54	99.76	1.50	
BP2	219.30	177.74	148.03	145.22	127.70	111.63	88.71	1.30	

Table: Effective cross section obtained after each cut for both signal ($2\ell^\pm + 4j + \cancel{E}_T$) and background and the respective required integrated luminosity for 5σ significance at 13 TeV LHC.

$2\ell^\pm + 4j + \cancel{E}_T$

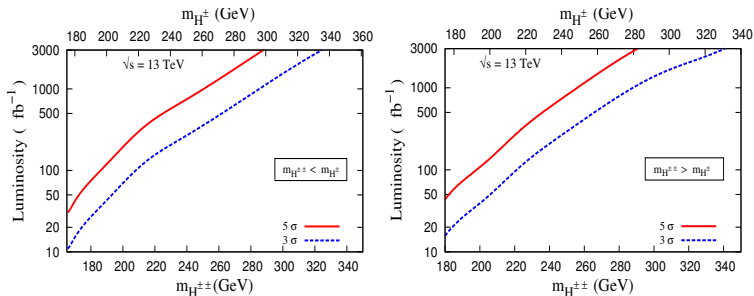


Figure: Left (Right) panel shows the required integrated luminosity for $2\ell^\pm + 4j + \cancel{E}_T$ final state with respect to charged Higgs masses at the LHC at $\sqrt{s} = 13$ TeV for positive (negative) scenario.

Conclusion

- We have found that the additional scalar fields can certainly surmount the instability problem and provide us with an absolutely stable vacuum even up to the Planck scale.
- We have chosen two distinct values of the triplet vev v_t (1 and 3 GeV) and have observed that the requirement of an absolutely stable vacuum up to the high Planck scale have pushed the neutral scalar mixing angle (α) to a quite small range of value for the non-degenerate mass scenario ($m_H(m_A) \gg m_h$) and peaks around a small positive value for considerably large m_H .
- Depending on the mass hierarchy, two possible scenarios (positive and negative) exist which however, at the end, yielded similar signal significance. In the allowed parameter space, with appreciable production cross section, the masses of the charged scalar can presumably be chosen around 200 GeV.
- Two specific final states at the collider, $(3\ell^\pm + \cancel{E}_T)$ and $(2\ell^\pm + 4j + \cancel{E}_T)$ at the 13 TeV LHC run. A proper cut-based analysis with detector simulation reveals that the first channel can only be probed at the 13 TeV LHC with high integrated luminosity around 1200 fb^{-1} and should be promoted for a HL-LHC. On the other hand, for the second channel we have found that even a 5σ discovery reach is possible with the present LHC data with only around 40 fb^{-1} luminosity.
- We have not taken into account different experimental issues arising from the electron charge misidentification, jet faking as leptons and photon conversion into lepton pair.

- The misidentification probability of a jet to be an isolated electron is around $(0.1 - 0.2)\%$ for $p_T \simeq 30$ GeV.
- This would imply that for the $3\ell + \cancel{E}_T$ and $2\ell + 4j + \cancel{E}_T$ signal channels, all the SM multi-jet background processes will be down by order 10^{-9} and 10^{-6} respectively.
- The electron misidentification probability is also very small $\mathcal{O}(0.1\%)$ in the central rapidity region.



Here, we will present the one loop RGEs of all the relevant couplings (gauge, Yukawa and scalar quartic couplings) of the Type-II seesaw model[M. A. Schmidt et al, PhysRevD.76.073010]. For convenience, we introduce the shorthand notation $\mathcal{D} \equiv 16\pi^2 \frac{d}{d(\ln\mu)}$.

Gauge and top Yukawa couplings: The RGE for the gauge couplings,

$$\mathcal{D}g_1 = \frac{47}{10}g_1^3, \quad (22a)$$

$$\mathcal{D}g_2 = -\frac{5}{2}g_2^3, \quad (22b)$$

$$\mathcal{D}g_3 = -7g_3^3. \quad (22c)$$

The RGE for the top Yukawa coupling,

$$\mathcal{D}y_t = y_t \left(\frac{9}{2}y_t^2 - \left(8g_3^2 + \frac{9}{4}g_2^2 + \frac{17}{20}g_1^2 \right) \right), \quad (22d)$$

where, $g_1 = \sqrt{\frac{5}{3}}g'$ with GUT renormalization.

Scalar quartic couplings: We express the RGEs of the scalar quartic coupling with a redefinition of the coupling to match with the potential notation of Ref. [?] which can

be translated from our notation in the following way.

$$\Lambda_0 = \frac{\lambda}{2}, \quad (23a)$$

$$\Lambda_1 = 2\lambda_2 + 2\lambda_3, \quad (23b)$$

$$\Lambda_2 = -2\lambda_3, \quad (23c)$$

$$\Lambda_4 = \lambda_1 + \frac{\lambda_4}{2}, \quad (23d)$$

$$\Lambda_5 = -\frac{\lambda_4}{2}. \quad (23e)$$

The RGEs for the five quartic couplings that appear are then given by,

$$\mathcal{D}\Lambda_i = \beta_{\Lambda_i} + G_i, \quad (i = 0, 1, 2, 4, 5), \quad (24)$$

where, β_{Λ_i} and G_i are as follows:

$$\beta_{\Lambda_0} = 12\Lambda_0^2 + 6\Lambda_4^2 + 4\Lambda_5^2, \quad (25a)$$

$$\beta_{\Lambda_1} = 14\Lambda_1^2 + 4\Lambda_1\Lambda_2 + 2\Lambda_2^2 + 4\Lambda_4^2 + 4\Lambda_5^2, \quad (25b)$$

$$\beta_{\Lambda_2} = 3\Lambda_2^2 + 12\Lambda_1\Lambda_2 - 8\Lambda_5^2, \quad (25c)$$

$$\beta_{\Lambda_4} = \Lambda_4 (8\Lambda_1 + 2\Lambda_2 + 6\Lambda_0 + 4\Lambda_4 + 8\Lambda_5^2), \quad (25d)$$

$$\beta_{\Lambda_5} = \Lambda_5 (2\Lambda_1 - 2\Lambda_2 + 2\Lambda_0 + 8\Lambda_4), \quad (25e)$$

and,

$$G_0 = \left(12y_t^2 - \left(\frac{9}{5}g_1^2 + 9g_2^2 \right) \right) \Lambda_0 + \frac{9}{4} \left(\frac{3}{25}g_1^4 + \frac{2}{5}g_1^2g_2^2 + g_2^4 \right) - 12y_t^4 \quad (26a)$$

$$G_1 = - \left(\frac{36}{5}g_1^2 + 24g_2^2 \right) \Lambda_1 + \frac{108}{25}g_1^4 + 18g_2^4 + \frac{72}{5}g_1^2g_2^2, \quad (26b)$$

$$G_2 = - \left(\frac{36}{5}g_1^2 + 24g_2^2 \right) \Lambda_2 + 12g_2^4 - \frac{144}{5}g_1^2g_2^2, \quad (26c)$$

$$G_4 = \left(6y_t^2 - \left(\frac{9}{2}g_1^2 + \frac{33}{2}g_2^2 \right) \right) \Lambda_4 + \frac{27}{25}g_1^4 + 6g_2^4, \quad (26d)$$

$$G_5 = \left(6y_t^2 - \left(\frac{9}{2}g_1^2 + \frac{33}{2}g_2^2 \right) \right) \Lambda_5 - \frac{18}{5}g_1^2g_2^2. \quad (26e)$$

High Scale stability

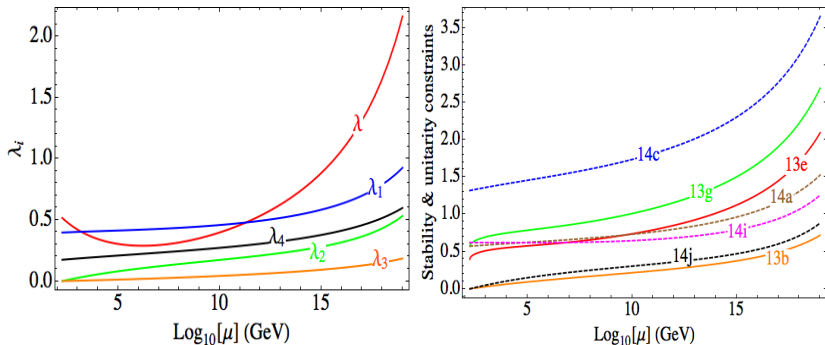


Figure: (Left panel) The running of the five scalar quartic couplings up to the Planck scale for the benchmark point BP1 of positive scenario. (Right panel) The running of some of the stability and unitarity constraints indicated by the corresponding equation numbers for the same benchmark point.